The AAPS Journal (2021) 23116
DOI: 10.1208/s12248-021-00647-0

Research Article

Pharmacokinetics of Monoclonal Antibody and Antibody Fragments in the Mouse Eye Following Systemic Administration

David Bussing[1] · Zhe Li[1] · Yingyi Li[1] · Hsuan-Ping Chang[1] · Hsueh-Yuan Chang[1] · Leiming Guo[1] · Ashwni Verma[1] · Dhaval K. Shah[1]

Received 30 March 2021; accepted 15 September 2021

Abstract. The ocular pharmacokinetics (PK) of antibody-based therapies are infrequently studied in mice due to the technical difficulties in working with the small murine eye. This study is the first of its kind to quantitatively measure the PK of variously sized proteins in the plasma, cornea/ICB, vitreous humor, retina, and posterior cup (including choroid) of the mouse and to evaluate the relationship between molecular weight (MW) and antibody biodistribution coefficient (BC) to the eye. Proteins analyzed include trastuzumab (150 kDa), trastuzumab-vc-MMAE (T-vc-MMAE, 155 kDa), $F(ab)_2$ (100 kDa), Fab (50 kDa), and scFv (27 kDa). As expected, ocular PK mirrored the systemic PK as plasma was the driving force for ocular exposure. For trastuzumab, T-vc-MMAE, $F(ab)_2$, Fab, and scFv, respectively, the BCs in the cornea/ICB were 0.610%, 0.475%, 1.74%, 3.39%, and 13.7%; the BCs in the vitreous humor were 0.0198%, 0.0427%, 0.0934%, 0.234%, and 5.56%; the BCs for the retina were 0.539%, 0.230%, 0.704%, 2.44%, and 20.4%; the BCs for the posterior cup were 0.557%, 0.650%, 1.47%, 4.06%, and 13.9%. The relationship between BC and MW was best characterized by a log–log regression in which BC decreased as MW increased, with every doubling in MW leading to a decrease in BC by a factor of 3.44×, 6.76×, 4.74×, and 3.43× in cornea/ICB, vitreous humor, retina, and posterior cup, respectively. In analyzing the disposition of protein therapeutics to the eye, these findings enhance our understanding of the potential for ocular toxicity of systemically administered protein therapeutics and may aid in the discovery of systemically administered protein therapeutics for ocular disorders.

KEY WORDS: ADC · antibody fragments · monoclonal antibody · mouse · ocular pharmacokinetics

INTRODUCTION

Monoclonal antibodies (mAbs) have become a well-established class of drug molecules with therapeutic indications ranging from chronic inflammation, infectious diseases, and many types of cancer (1). In 2020 alone, 10 mAb-based therapeutics were approved by the US Food and Drug Administration (FDA), despite the challenges posed by the COVID-19 pandemic (2). With a history of safety and a wide array of applications, investigators have also sought to take advantage of the modular nature of mAbs. Antibody fragments, such as fragment antigen binding (Fab, and the dimer $F(ab)_2$) and the single chain fragment variable (scFv) have been developed to take advantage of the highly specific nature of antibody-based therapies. Because of the smaller sizes of $F(ab)_2$ (100 kDa), Fab (50 kDa), and scFv (27 kDa), these fragments can reach target antigens deeper in tissues and tumors, and the lack of the fragment crystallizable (Fc) limits any unintended immune system activation (3). Additionally, antibody–drug conjugates (ADCs) are a rising class

Supplementary Information The online version contains supplementary material available at https://doi.org/10.1208/s12248-021-00647-0.

[1]Department of Pharmaceutical Sciences, School of Pharmacy and Pharmaceutical Sciences, The State University of New York at Buffalo, 455 Pharmacy Building, Buffalo, New York 14214-8033, USA
[2]To whom correspondence should be addressed. (e–mail: dshah4@buffalo.edu)

Published online: 08 November 2021

of antibody-based anticancer therapeutics, with 9 ADCs currently approved and over 100 more in clinical trials (4–8). Using the highly specific antibody, ADCs deliver a potent cytotoxic agent inside the antigen-expressing cancer cells, which eventually leads to cell death (9). As such, these molecules can theoretically minimizes off-target delivery of the cytotoxic drug molecules in healthy tissue (10).

Traditionally, the polar and large antibody-based protein therapeutics have been assumed to not enter into the ocular tissues at pharmacologically relevant levels after systemic administration. The eye is separated from the systemic circulation by the blood-retinal barrier (BRB) in the posterior segment and the blood-aqueous barrier (BAB) in the anterior segment (11). Moreover, the inner eye is an immune privileged space with an inherent immunosuppressive and anti-inflammatory environment (12, 13). However, despite the isolated nature of the eye, there is emerging evidence that antibody and antibody-based therapeutics such as ADCs may still pose a risk to ocular tissue, especially if the target antigen is expressed in the eye. In fact, adverse ocular events have been reported in multiple clinical trials of mAbs and ADC therapeutics following systemic administration (14–19). Smaller fragments such as $F(ab)_2$, Fab, and scFv have the potential to demonstrate even higher ocular toxicities following systemic administration due to their greater penetrative capabilities. However, the degree to which mAb, $F(ab)_2$, Fab, and scFv enter the eye following systemic administration has not been systemically investigated to date.

Furthermore, the current route of administration of protein therapeutics for ocular disease is via injection directly into the vitreous humor. The intravitreal (IVT) injection procedure is laborious for the ophthalmologist, stressful for the patient, and comes with a risk of developing secondary ocular pathologies (20, 21). As an alternative, the development of a systemically administered protein for a target in the eye would be a significant innovation in ophthalmology. Understanding the effect of physicochemical properties, such as molecular weight, on the ocular PK of proteins may help us devise a therapeutic strategy for eye disease using systemically administered antibody-based therapies.

Mouse models are a powerful tool in drug development, but they are not currently used in ocular PK research due to their small size, well-known anatomical differences between mice and humans, and the difficulty in collecting and separating ocular tissues. Instead, rabbits are the predominant species in existing literature on ocular PK of proteins (22, 23). Furthermore, rabbit models of human ocular diseases, such as dry eye, glaucoma, and age-related macular degeneration, are frequently used but are typically induced by investigators using invasive means (minor surgeries, application of toxic compounds, light-induced retinal damage, etc.) (24). However, in human, almost all nontraumatic and noninfectious ocular abnormalities are due to genetic components (25–27). Using mutant mouse models, the pathophysiology of inherited ocular diseases are better captured, and there are numerous mouse models of ocular disease ranging from retinal degeneration and neovascularization to cataracts and glaucoma (28–31). Techniques developed during this investigation overcome the technical difficulties of studying ocular PK in mouse models. We present here the experimental methods required to remove the mouse eye, separate the eye into separate tissues, and quantitate levels of exogenous antibody-based therapies in the ocular tissues.

To better understand the pharmacokinetics (PK) of protein therapeutics in the eye following systemic administration, here we have measured the exposure of five antibody-based therapeutics (trastuzumab (150 kDa), trastuzumab-vc-MMAE (T-vc-MMAE) (155 kDa), $F(ab)_2$ (100 kDa), Fab (50 kDa), and scFv (27 kDa)) in different ocular tissues of mice following intravenous administration. In addition, we have also explored the relationship between the size and ocular exposure of protein therapeutics in mice. All the protein therapeutics used in our investigation bind to human epidermal growth factor receptor 2 (HER2), and do not bind to any mouse antigen. Thus, any target mediated effect on the disposition of protein therapeutics has been eliminated from consideration. The ocular PK data presented here provides an unprecedented insight into the rate and extent of protein therapeutic exposure in different tissues of the eye following systemic administration, and how the size of a protein can affect this PK.

MATERIALS AND METHODS

Production and Characterization of Antibody, ADC, and Fragments

Trastuzumab (Herceptin; Genentech, South San Francisco, CA) was purchased from a local hospital in a commercially available package as a lyophilized powder that was reconstituted in accordance with instructions in the package insert (32). The antibody fragments of trastuzumab ($F(ab)_2$ (100 kDa), Fab (50 kDa), and scFV (27 kDa)) were generated in-house, as described in detail in our previous publication (33).

Preparation of ADC

Trastuzumab-vc-MMAE (T-vc-MMAE) was produced in-house by random conjugation of monomethyl auristatin E (MMAE) to inter-chain disulfide bonds using a valine-citrulline (vc) linker as reported previously (34, 35). Partial

reduction of the inter-chain disulfide bonds was achieved by incubation of trastuzumab with 2.5 molar equivalents of TCEP (tris(2-carboxymethyl) phosphine). Further incubation with 8 molar equivalents of vc-MMAE (maleimidocaproyl-val-cit-MMAE) resulted in an approximate drug-antibody ratio (DAR) of 4. T-vc-MMAE was separated from unconjugated vc-MMAE on a PD-10 desalting column containing Sephadex G-25 resin (GE Healthcare Life Sciences, Marlborough, MA). The final T-vc-MMAE product was characterized by high-performance liquid chromatography couple with ultraviolet detection (HPLC–UV). Aggregation in the final product was assessed by size-exclusion chromatography (SEC), and the distribution of different DAR species was determined by hydrophobic interaction chromatography (HIC).

Preparation of F(ab)$_2$ and Fab

The F(ab)$_2$ and Fab fragments of trastuzumab were prepared using commercially available kits (Thermo Fisher Scientific, Waltham, MA). Briefly, trastuzumab was purified using a Zeba Spin Desalting column (Thermo Fisher Scientific) and incubated in a microcentrifuge tube with either (1) pepsin-immobilized resin in digestion buffer at 37 °C for 8 h to generate F(ab)$_2$ or (2) papain-immobilized resin in digestion buffer at 37 °C for 12 h to generate Fab. The digestion products were separated from their respective resins by centrifugation. Both the F(ab)$_2$ digestion mixture and Fab digestion mixture were purified separately on a Bio-Rad HGC System using a hydroxyapatite column (Bio-Rad, Hercules, CA). Separation for each fragment was optimized by changing the gradient of two eluent buffers: buffer A containing 10 mM sodium phosphate and 5 ppm calcium chloride, pH 6.5, and buffer B containing 500 mM sodium phosphate and 5 ppm calcium chloride, pH 6.5. The peaks from the chromatogram were identified using gel electrophoresis (SDS-PAGE). The final products were buffer exchanged in PBS prior to *in vivo* experiments.

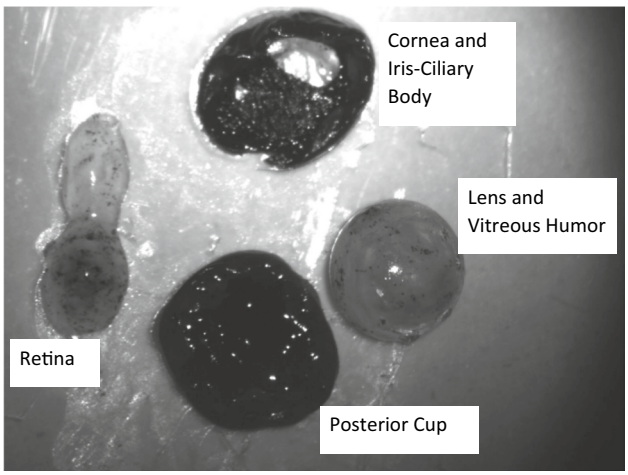

Fig. 1 Ocular tissues from mouse eye after separation into four major components. These tissues were further homogenized for the measurement of drug concentrations. The lens and vitreous humor undergo further separation to isolate the vitreous fluid

Preparation of scFV

The scFv plasmid sequence was designed by linking the VH and VL region sequences of trastuzumab with a polyglycine linker $(GGGGS)_3$. The plasmid contained a restriction enzyme site for NheI at the beginning of the sequence a site for BamHI at the end. Plasmid was synthesized by Genscript (Nanjing, China). Double enzyme restriction for the scFv plasmid and pcDNA5_FRT expression plasmid was performed with NheI and BamHI (New England Biolabs, Ipswich, MA) at 37 °C for 2–4 h. Subsequently, the cDNA products for the plasmid were collected and ligated using the T4 ligation system (QIAGEN, Hilden, German) by incubating them at 16 °C for 1–2 h. The ligated plasmid, scFv-FRT, was transfected into TOP10 chemically competent *Escherichia coli* cells (Invitrogen, Waltham, WA) for amplification. Plasmid was extracted from the *E. coli* using the Plasmid Mini Kit (QIAGEN) and transfected into Chinese hamster ovary (CHO) cells. Cho cells were transfected with the scFv-FRT plasmid and the pOG44 plasmid (Invitrogen) and underwent two rounds of subcloning in 96-well plates to separate single cells. The best monoclones were determined by an ELISA for scFv in the supernatant of each well. Two clones were selected for amplification in T-75 flasks using SFM-CD CHO media. After ~ 10 days, the cell culture was highly confluent, and the supernatant was collected. The scFv was purified using a His GraviTrap column (GE Healthcare Life Sciences, Chicago, IL) and confirmed with SDS-PAGE analysis and Western blotting analysis. The final products were buffer exchanged in PBS prior to *in vivo* experiments.

Ocular Tissue Preparation for Analysis

Removal and Dissection of Ocular Tissues

Eyes were enucleated from mice following methods established by Aers et al. (36). Briefly, forceps are used to coax the eye from the socket and clamp the optic nerve. Then, the mouse is moved in a circular motion against the operating table until the eyeball is removed. Using this method, the eye is easily removed with little to no bleeding, which minimizes contamination of the ocular tissue with blood. The individual eyes are stored in separate tubes at – 80 °C until dissection and analysis. Under a dissection microscope, the eyes are separated into 4 constitutive components: the cornea/ICB, the lens capsule (contains lens and vitreous

humor), the retina, and the posterior cup (Fig. 1). First, an incision is made at the limbus with curved micro scissors, and the cut is continued around the orbit to separate the cornea and ICB together. The lens capsule is then easily removed. Holding the remaining tissues with micro forceps, the retina can be pulled away from the posterior cup with a second pair of micro forceps. The posterior cup contains the choroid, sclera, and untrimmed connective tissue. With clean micro scissors, the cornea/ICB and posterior cup were cut into smaller pieces prior to being placed in microcentrifuge tubes for homogenization. Tissues from both the left and right eyes were pooled to allow for minimal dilution of the sample prior to ELISA.

Homogenization of Solid Ocular Tissues

For the cornea/ICB, retina, and posterior cup, tissues were weighed and homogenized in 3:1 v/w Pierce® RIPA Buffer (Thermo Fisher Scientific) containing 1 × Halt™ Protease Inhibitor Cocktail (Thermo Fisher Scientific). The homogenization process used a Fisherbrand™ Model 120 Sonic Dismembrator (Fisher Scientific) with a 1/8″ probe. Tissues underwent three cycles of sonication of 3 s on and 5 s off with a sonication amplitude set to 45%. Samples were stored at − 20 °C until analysis.

Separation of Vitreous Humor

The lens capsule obtained after dissection contains both the lens and vitreous humor. In a microcentrifuge tube, the lens capsule was combined with 5 µL of Pierce® RIPA Buffer with 1 × Halt™ Protease Inhibitor Cocktail and sonicated for a single 3-s pulse with an amplitude of 20% to disrupt the capsule. The tubes were centrifuged at 1800 g for 15 min to separate the dense lens from the supernatant containing the vitreous humor. The supernatant was collected, the volume of vitreous humor calculated, and RIPA + Halt buffer added for a final ratio of 3:1 v/w buffer to vitreous humor. Samples were stored at − 20 °C until analysis.

ELISA Development for Antibody and Fragments

ELISA Method to Quantify Trastuzumab, F(ab)$_2$, and Fab in Ocular Tissues

Eyes obtained from C57BL/6 J mice were used to build standard curves for trastuzumab, T-vc-MMAE, F(ab)$_2$, and Fab in 40 × matrix dilutions. For trastuzumab and T-vc-MMAE analysis, goat anti-human IgG (Fc specific, cross-adsorbed) F(ab)$_2$ (Bethyl Laboratories, Montgomery, TX) was used for coating. For F(ab)$_2$ and Fab analysis, goat anti-human IgG (F(ab)$_2$ specific, cross adsorbed) F(ab)$_2$ (Bethyl) was used for coating. The coating antibodies were diluted to 5 µg/mL in 20 mM Na_2HPO_4. Nunc Maxisorp 384-well plates were incubated with 35 µL/well diluted coating antibody at 4 °C overnight. Plates were warmed to room temperature and washed three times with 1 × PBS-Tween 20 (0.05%) and three washes with deionized water. Plates were blocked with 90 µL/well 1% BSA at room temperature for 1 h before washing. Serial dilutions of trastuzumab, F(ab)$_2$, or Fab ranging from 250 to 0.122 ng/mL were added as standards in triplicate (30 µL/well), and plates were incubated at room temperature for 2 h. Plates were washed, and 30 µL/well of goat anti-human IgG (F(ab)$_2$ specific, AP-conjugated, cross adsorbed) F(ab)$_2$ (Bethyl) (2500 × dilution in 1 × PBS-Tween 20 (0.05%)) was added to each well for incubation at room temperature for 1 h. After a final wash, 60 µL p-nitro phenyl phosphate (1 mg/mL in 1 × diethanolamine buffer) was added to each well, and the plate was read immediately. The change in absorbance at 405 nm was recorded over time with a FilterMax™ F5 microplate reader (Molecular Devices, San Jose, CA). Data was interpreted with a 5-paramter standard curve using the included SoftMax® Pro software (Molecular Devices).

ELISA Method to Quantify scFv in Ocular Tissues

The ELISA procedure was the same as described above. However, recombinant human HER2-Fc fusion protein (Sino Biological, Beijing, China) was coated on the plate (35 µL at 5 µg/mL) to capture scFv. Anti-6X His tag antibody (HRP-conjugated, Abcam, Cambridge, UK) was used as the detection antibody (30 µL of 10,000 × dilution). TMB (3,3′,5,5′-tetramethylbenzidine) ELISA substate solution (Thermo Fisher Scientific) was added to each well, and the change in absorbance at 405 nm was monitored as described above.

ELISA Method to Quantify Trastuzumab, T-vc-MMAE, F(ab)$_2$, Fab, and scFv in Plasma

The ELISA methods for detection of the proteins of interest mouse plasma are described in detail in Li et al. (33). The procedure is the same as described above with three differences: (1) standard curves were generated with plasma dilutions of 300 × for trastuzumab and T-vc-MMAE, 300 × for F(ab)$_2$, 50 × for Fab, and 10 × for scFv; (2) serial dilutions for standards ranged from 1000 to 3.9 ng/mL; and (3) goat anti-human IgG (F(ab)$_2$ specific, cross adsorbed) F(ab)$_2$ (Bethyl) was used to capture IgG.

***In vivo* PK Study**

All animal procedures were approved by the Institutional Animal Care and Use Committee at the State University of New York at Buffalo. Ocular samples were collected

alongside the studies carried out in Li et al. (2019) in MDA-MB-468 tumor bearing nude mice (33). Trastuzumab, $F(ab)_2$, Fab, and scFv were each administered by penile vein injection at a dose of 10 mg/kg. Four terminal sampling time points of three mice each were selected for each protein. For trastuzumab, samples were collected at 6, 24, 72, and 168 h. For $F(ab)_2$, samples were collected at 1, 6, 24, and 48 h. For Fab, samples were collected at 10 min and 1, 4, and 24 h. For scFv, samples were collected at 5 min and 1, 4, and 24 h. The T-vc-MMAE PK study was carried out separately in N87 tumor bearing nude mice that received a 10 mg/kg dose of the ADC by penile vein injection. Terminal samples were collected at 10 min and 6, 24, 72, and 168 h. At each time point, blood was collected by cardiac puncture, and plasma separated by centrifugation (2000 g for 20 min) and stored at − 80 °C. Both eyes were enucleated as described above and stored in individual microcentrifuge tubes at − 80 °C until dissection.

Data Analysis

Areas under the concentration time curves until the last time point ($AUC_{0\text{-last}}$) for all analytes were calculated by non-compartmental analysis in MATLAB 2020b using SimBiology 6.0 (37). The standard deviations around mean AUC values were calculated using the modified Bailer method implemented in Microsoft Excel (38, 39). Statistical significance was determined using the Student's *t*-test (two-tailed) with a threshold *p* value of less than 0.05. The relationship between biodistribution coefficient (BC) and molecular weight (in kDA) was characterized by curve fitting with several equations using the Curve Fitting Toolbox 3.5.12 in MatLab 2020b (40). Goodness of fit was evaluated by visual inspection and R^2 values. The equation with the highest overall R^2 value across the ocular tissues was considered the most accurate. The best fitting equation is the following log–log regression model:

$$\ln(BC) = \ln(a) - b * \ln(MW) \quad (1)$$

$$BC = \frac{AUC_{0-last_{tissue}}}{AUC_{0-last_{plasma}}} * 100\% \quad (2)$$

RESULTS

Development of ELISA Methods to Quantify Antibody and Fragments in Ocular Tissues

Supplemental Figs. 1–5 show typical ELISA standard curves for trastuzumab, T-vc-MMAE, $F(ab)_2$, Fab, and scFv in the ocular matrices. Standard curves utilizing the 5-parameter equation had R^2 values of ≥ 0.95 in the SoftMax® Pro software. Intra-day and inter-day variability for all the ELISA methods is presented in Supplemental Table I. ELISAs allowed for quantification of trastuzumab and scFv with a lower limit of 0.488 ng/mL, and for quantification of $F(ab)_2$ and Fab with a lower limit of quantitation of 0.122 ng/mL.

Pharmacokinetics of trastuzumab, ADC, $F(ab)_2$, Fab, and scFv in Mouse Plasma and Ocular Tissues

Figure 2A shows the observed PK of trastuzumab (150 kDa) in mouse plasma and ocular tissues. Concentrations in the plasma are significantly higher than ocular tissues as expected due to the BRB, which isolates the eye from the systemic circulation. Interestingly, concentrations in the retina were equivalent to levels seen in the more vascularized ocular tissues in the posterior cup and cornea/ICB. However, the barrier properties in the eye are particularly apparent in the extremely low levels of trastuzumab seen in the vitreous humor, which is isolated from the systemic circulation by both the BRB in the posterior segment of the eye and the BAB in the anterior segment of the eye. All ocular tissues saw < 1% exposure to trastuzumab compared to the systemic circulation, with exposure in the vitreous humor being lowest at 0.0198% of plasma levels (Table I).

The ADC, T-vc-MMAE (155 kDa), shows a similar PK profile as the parent antibody, trastuzumab (Fig. 2b). Again, the plasma levels of T-vc-MMAE are significantly higher than those in the ocular tissues. The retina and posterior cup show more pronounced absorption phases than seen with trastuzumab, but all tissues mirror the plasma profile in the terminal phase. Just as with trastuzumab, the vitreous humor shows the lowest levels of T-vc-MMAE. Exposure in the ocular tissues compared to plasma were consistent with results seen for trastuzumab (Table I); all tissues had < 1% of T-vc-MMAE exposure compared to plasma. The absolute exposure of T-vc-MMAE and trastuzumab are similar in plasma, cornea/ICB, and posterior cup, but there was a significant twofold higher exposure of T-vc-MMAE in the vitreous humor compared to trastuzumab ($p < 0.05$) and a twofold lesser exposure in the retina ($p < 0.05$) (Table II).

The PK of $F(ab)_2$ (100 kDa) (Fig. 2c) shows a similar trend with higher levels of $F(ab)_2$ in the plasma over the ocular tissues. Again, concentrations in the solid tissues are very similar at early time points, with some apparent accumulation in cornea/ICB that is followed by a slower release. Concentrations of $F(ab)_2$ are lowest in the vitreous humor and are similar to the 150 kDa trastuzumab in the first 24 h. $F(ab)_2$ in the vitreous and plasma was BLQ at 48 h. Exposure in the ocular tissues was between 1.74 and 0.0934% of plasma exposure (Table I).

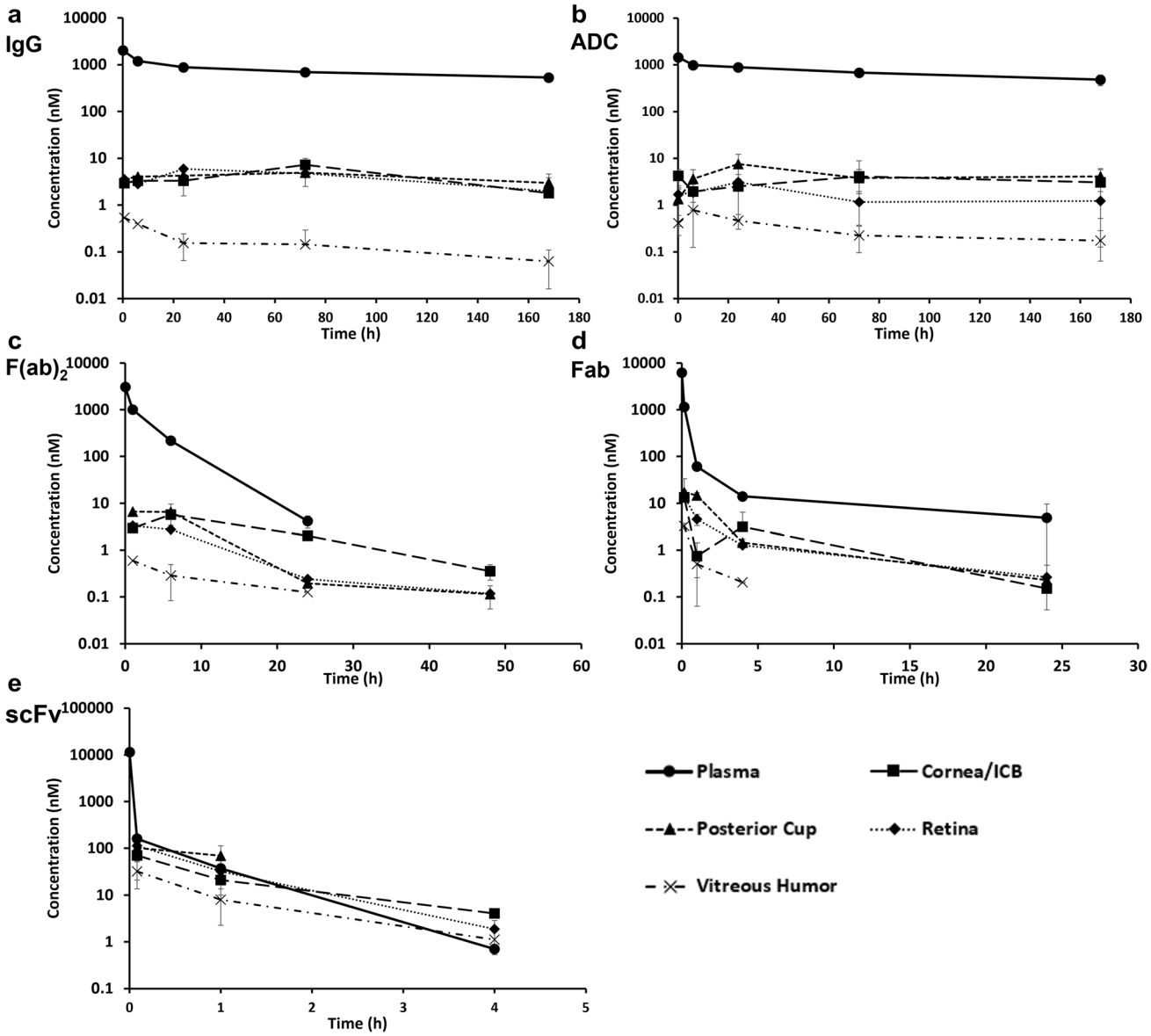

Fig. 2 Observed pharmacokinetics of **a** trastuzumab (IgG), **b** T-vc-MMAE (ADC), **c** $F(ab)_2$, **d** Fab, and **e** scFv in the plasma, cornea/ICB, vitreous humor, retina, and posterior cup after 10 mg/kg IV dosing

Table I Biodistribution Coefficients (i.e., Tissue/Plasma $AUC_{0\text{-last}}$ Ratios as %) of Antibody-Based Therapeutics in Ocular Tissues

	BC(%)			
	Cornea/ICB	Vitreous humor	Retina	Posterior cup
Trastuzumab	0.610	0.0198	0.539	0.557
T-vc-MMAE	0.475	0.0427	0.230	0.650
$F(ab)_2$	1.74	0.0934	0.704	1.47
Fab	3.39	0.234	2.44	4.06
scFv	13.7	5.56	20.4	13.9

For Fab (50 kDa) (Fig. 2d), concentrations in the tissues, while lower than levels in plasma, are much closer to concentrations in the systemic circulation than is seen with the larger trastuzumab and $F(ab)_2$ molecules. In this case, Fab PK in the eye parallels the PK in plasma with the exception of the cornea/ICB, which shows a rapid drop between 10 min and 1 h before an apparent accumulation of Fab by 4 h. The change may signify the movement of Fab from the vascular space of the tissue to the interstitial compartment and accumulation. The relative exposure of the 50 kDa Fab in the ocular tissues was 2- to 3.4-fold higher than that of the 100 kDa $F(ab)_2$, with exposure in the posterior cup reaching 4.06% of plasma levels (Table I).

Table II $AUC_{0\text{-last}}$ of Antibody-Based Therapeutics in Ocular Tissues

	$AUC_{0\text{-last}}$ (nM*h)				
	Plasma	Cornea/ICB	Vitreous Humor	Retina	Posterior Cup
Trastuzumab	125,000	763	24.8[a]	674[b]	696
T-vc-MMAE	118,000	562	50.5[a]	273[b]	768
$F(ab)_2$	7060	123	6.59	49.7	57.3
Fab	1410	47.8	3.30	34.4	87.3
scFv	627	85.8	34.9	128	768

[a,b] Significant difference in AUCs between trastuzumab and T-vc-MMAE ($p < 0.05$)

Table III Estimated Parameters for the BC *vs* MW Relationship Shown in Fig. 3

	$\ln(BC) = \ln(a) - b * \ln(MW)$		
Tissue	$\ln(a)$	b	R2
Cornea/ICB	8.42	1.78	0.97
Vitreous humor	10.3	2.76	0.92
Retina	10.1	2.24	0.95
Posterior cup	8.46	1.78	0.99

Figure 2e shows the PK of scFv (27 kDa), which shows several remarkable properties. Firstly, initial concentrations of scFv in ocular tissues at 5 min are very close to plasma levels, and concentrations in the cornea/ICB, retina, and posterior cup are equivalent to plasma concentrations after 1 h. By hour 4, all tissue concentrations are higher than plasma, indicating presence of scFv in the interior of these tissues. These results suggest that smaller protein therapeutics like scFv and domain antibodies could be potentially therapeutic molecules for ocular disease following systemic administration and may provide a pathway to avoid direct ocular injection of protein therapeutics. Remarkably, scFv exposure reached 20.4% of plasma exposure in the retina (Table I).

Overall, all the proteins evaluated here showed a rapid distribution to the eyes with a PK that is parallel to that of plasma after initial time points. Vitreous humor concentrations were consistently lower than the concentrations in other vascularized ocular tissues. Among these tissues, exposure was typically highest in the cornea/ICB and posterior cup, followed by the retina. In Fig. 3, we have compiled the exposure data for all the molecules in all ocular tissues and have established a quantitative relationship between biodistribution coefficient (BC) values (derived from $AUC_{tissue}/AUC_{plasma}$ ratios) and protein size (40, 41). We found that there was a clear trend between molecular size and the extent of protein distribution to the ocular tissues that is quantitatively characterized using the log–log regression equation (Eq. 1) with the parameter estimates for the independent variables, a and b, listed in Table III. The parameter a can be interpreted as the BC of a hypothetical protein with a MW of 1 kDa (i.e., $\ln(MW) = 0$). The parameter b represents the rate of decrease in BC as the protein MW increases. The vitreous humor had the highest b parameter value ($b = 2.76$) which is reflected in Fig. 3 by the more pronounced decrease in BC as the MW increases. Overall, a significant relationship between the BC value and MW was observed with each reduction in size from 155 to 27 kDa with every doubling in the MW leading to a corresponding decrease in BC by a factor of 3.44×, 6.76×, 4.74×, and 3.43× in cornea/ICB, vitreous humor, retina, and posterior cup, respectively.

DISCUSSION

In this manuscript, we have presented the first study that quantitatively and systemically examines the PK of a mAb, an ADC, an $F(ab)_2$, an Fab, and an scFv in the ocular tissues of mice following systemic administration. In addition, we have sought to establish a quantitative relationship between the size of protein therapeutics and the extent of their distribution in ocular tissues. To accomplish our goals, we have developed an experimental system for collection of very small ocular tissues from mouse eyes and have developed sensitive and specific ELISA methods for quantification of IgG, $F(ab)_2$, Fab, and scFv in ocular tissue of mice.

Quantitative studies such as the one presented here are limited by the physiology of the eye and experimental constraints. Concentrations in the ocular tissues are expected to be low due to the presence of two main barriers in the eye. The BRB and the BAB separate the ocular tissues from the systemic circulation by tight epithelial layers and numerous transport systems (11). Moreover, the size of the mouse eye is very small at an average of 16.7 mg (in-house data). With the extremely small amounts of tissue obtained after dissection of the mouse eyes and low partitioning of large molecular weight proteins into the eye, dilution of the samples must be kept to a minimum. In a study with systemic administration, the eyes may be pooled to alleviate the problem of small sample volume. However, it is of great importance to have highly sensitive assays for the proteins of interest to accommodate these challenges. With an ELISA utilizing the 384-well plate format, the proteins

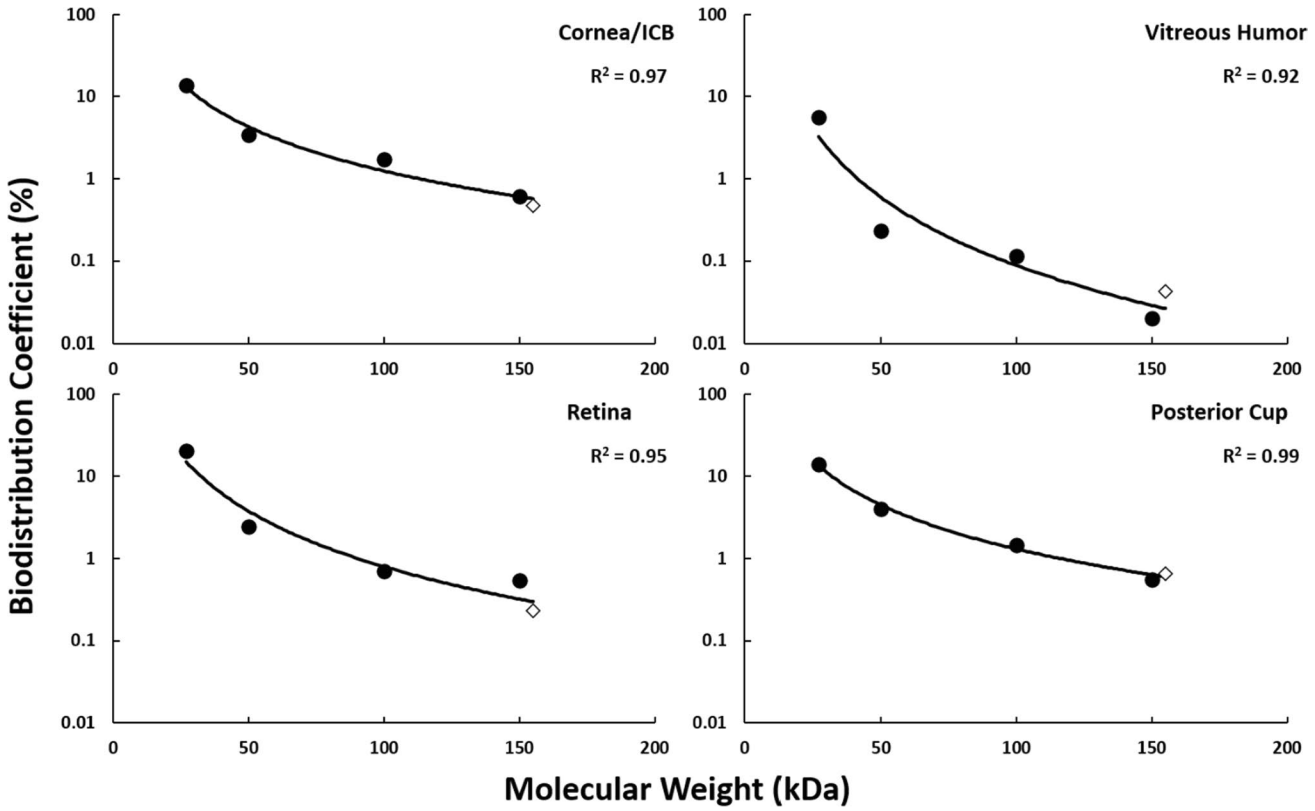

Fig. 3 Quantitative relationship between biodistribution coefficient values for cornea/ICB, vitreous humor, retina, and posterior cup and molecular weight of antibody-based therapeutics in kDa (black circle - IgG, $F(ab)_2$, Fab, scFv; diamond - T-vc-MMAE). The solid black line represents fitted BC *vs* MW for each tissue. Parameters of the log–log regression are shown in Table III, and goodness of fit is represented by R^2 values

used in this study could be detected at the sub-ng/mL level while using a minimal (30 μL/well in triplicate) volume of prepared sample.

The biologics used in this study were based on the trastuzumab molecule, which targets human epidermal growth factor receptor 2 (HER2) but has no cross-reactive target in mice (42, 43). Therefore, target mediated effects are not seen in the data. The PK of antibodies and fragments are well studied after intravitreal (IVT) administration in rabbits and monkeys (44–52). After IVT dosing, a monoclonal antibody or fragment rapidly appears in the aqueous humor, ICB, and retina and appears slowly in plasma as the molecule exits the eye (47–52). Typically, the PK profile of the ocular tissues mirror that of the vitreous humor as large molecules are rate limited by elimination from the vitreous. However, as seen in Fig. 2, the plasma PK dictates the PK in the posterior cup, retina, and vitreous humor when the protein is administered IV. Interestingly, the cornea/ICB show some accumulation of protein in the trastuzumab, T-vc-MMAE, $F(ab)_2$, and Fab profiles. One explanation for this phenomena could be that the therapeutic in the vitreous is eliminated by the anterior route of elimination, and the delayed C_{max} in the cornea/ICB is due to the time it takes for the molecule to move to the front of the eye. Interestingly, the cornea/ICB profiles for T-vc-MMAE and Fab show sharp initial declines mirroring the plasma profile followed by subsequent increase. The initial decline may indicate that the T-vc-MMAE or Fab is primarily in the vascular space of the cornea/ICB, and the subsequent rise is due to penetration of the protein into the extracellular or even cellular space.

When looking at the exposure relationships between the different molecules, a clear trend is observed with smaller molecular weight formats having greater partitioning into the ocular tissues. The largest molecules, 150 kDa trastuzumab and 155 kDa T-vc-MMAE, have the smallest degree of tissue partitioning with cornea/ICB, retina, and posterior cup having BC values ranging from 0.539 to 0.610% for trastuzumab and 0.475 to 0.650% for T-vc-MMAE. The vitreous humor had BC value of 0.0198% and 0.0427% for trastuzumab and T-vc-MMAE, respectively. It is very interesting to note that these BC values are the lowest reported values for any molecule in any tissue so far, and even lower than the reported BC value of ~ 0.3% for antibodies in the brain (40, 53). For the 100 kDa $F(ab)_2$, BC value in the ocular tissues increased to 1.74% for cornea/ICB, 0.704% for retina, 1.47% for posterior cup, and 0.0934% for vitreous

humor. On average, relative exposure increased 2.88-fold with the change from 150 to 100 kDa. For the 50 kDa Fab molecule, BC values again increased, with 3.39% for cornea/ICB, 2.44% for retina, 4.06% for posterior cup, and 0.234% for vitreous humor. In this case, relative exposure increased 2.67-fold with the change from 100 to 50 kDa. Lastly, the 27 kDa scFv showed the most dramatic increase in BC values with 13.7% for cornea/ICB, 20.4% for retina, 13.9% for posterior cup, and 5.56% for the vitreous humor. Overall, these data suggest that the smaller molecular size proteins are able to better penetrate through the ocular barriers to achieve greater exposures into the eye.

On an absolute exposure basis, the $AUC_{0\text{-}t\_last}$ showed a positive correlation with molecular weight. Among trastuzumab, T-vc-MMAE, $F(ab)_2$, and Fab, the absolute exposure in all the ocular tissues is greatest for trastuzumab (Table II). The high absolute exposure of trastuzumab and T-vc-MMAE is likely due to FcRn mediated recycling in the local tissues, and the long systemic exposure of exogenous mAb, which drives the partitioning into the ocular tissues. Notably, significant differences in vitreal AUC and retinal AUC between trastuzumab and T-vc-MMAE suggest a possible influence of the lipophilic MMAE in disposition to these tissues. Comparing scFv and Fab shows an inverse correlation between size and absolute exposure. In this case, absolute exposure of scFv was higher than that seen with Fab, highlighting the ability of scFv to penetrate more in ocular tissues. Such high exposure of scFv in the ocular tissues reveals it to be a potential candidate for the systemic treatment of ocular disease. The primary barrier to systemic treatment with scFv is its rapid elimination and short half-life in the systemic circulation. However, with an appropriate delivery device, slow release formulation, or fusion with a modality that binds to albumin/FcRn, the potential for scFv to reach the site-of-action within the eye can be accomplished. It is also important to mention that following systemic administration of protein therapeutics, a significant fraction of injected dose will also distribute to tissues other than the ocular tissue. This may lead to unintended pharmacological consequences if the target is not selectively overexpressed in the eye and the therapeutic index of the protein therapeutic is very low.

The high absolute exposures of trastuzumab and T-vc-MMAE in ocular tissues support the potential for toxicity of mAbs and ADCs delivered systemically, especially if target antigen is expressed in the eye. The highly potent ADCs pose a particular risk for ocular toxicity. Indeed, ocular adverse events of ADCs containing maytansines or monomethyl auristatin F have been observed in numerous clinical trials (19).

While findings from this study are limited to IgG, $F(ab)_2$, Fab, and scFv, the large size range covered (27 to 150 kDa) helps us establish a quantitative relationship between molecular weight and the extent of exposure in the ocular tissues. However, due to the non-binding nature of trastuzumab in mice, the effect of target mediated drug disposition (TMDD) on the systemic exposure, and in turn the ocular exposure, of these moieties is not accounted for (54, 55). Furthermore, our results may not be translatable to other large molecule therapeutics, such as liposomes, PEGylated proteins, and gene therapies. It also remains to be seen if the unprecedented observations made by us in the presented mouse study can be translated to other animal species and human.

CONCLUSION

In summary, here we have developed highly sensitive ELISA methods for quantification of IgG, $F(ab)_2$, Fab, and scFv in the ocular tissues of mice (i.e., cornea/ICB, vitreous humor, retina, and posterior cup). We have characterized the PK of trastuzumab, T-vc-MMAE, $F(ab)_2$, Fab, and scFv in the mouse eye following systemic administration and have established an inverse relationship between molecular weight and the exposure of protein therapeutics in ocular tissues. In conjunction with genetic mouse models of ocular diseases, the experimental techniques presented here open the door to further study of protein therapies to treat ocular disease in preclinical species. Ultimately, the findings presented here paves the way for enhanced understanding of the ocular toxicity of systemically delivered protein therapeutics and may facilitate the discovery of systemically administered protein therapeutics for ocular disorders.

Funding This project was partially funded by the Center for Protein Therapeutics (CPT) at the University at Buffalo (UB). D.K.S is supported by NIH grants GM114179, AI138195, and R01CA246785.

References

1. Lu RM, Hwang YC, Liu IJ, Lee CC, Tsai HZ, Li HJ, *et al*. Development of therapeutic antibodies for the treatment of diseases. J Biomed Sci. 2020;27(1):1.
2. Kaplon H, Reichert JM. Antibodies to watch in 2021. MAbs. 2021;13(1):1860476.
3. Bates A, Power CA. David *vs.* Goliath: the structure, function, and clinical prospects of antibody fragments. Antibodies (Basel). 2019;8(2).
4. Chau CH, Steeg PS, Figg WD. Antibody-drug conjugates for cancer. Lancet. 2019;394(10200):793–804.
5. Collins DM, Bossenmaier B, Kollmorgen G, Niederfellner G. Acquired resistance to antibody-drug conjugates. Cancers (Basel). 2019;11(3).
6. Mullard A. 2019 FDA drug approvals. Nat Rev Drug Discov. 2020;19(2):79–84.
7. FDA approves new treatment option for patients with HER2-positive breast cancer who have progressed on available therapies

[press release]. U.S. Food and Drug Administration, December 20, 2019.
8. FDA approves new therapy for triple negative breast cancer that has spread, not responded to other treatments [press release]. U.S. Food and Drug Administration, April 22, 2020.
9. Kalim M, Chen J, Wang S, Lin C, Ullah S, Liang K, *et al*. Intracellular trafficking of new anticancer therapeutics: antibody-drug conjugates. Drug Des Devel Ther. 2017;11:2265–76.
10. Lambert JM, Morris CQ. Antibody-drug conjugates (ADCs) for personalized treatment of solid tumors: a review. Adv Ther. 2017;34(5):1015–35.
11 Kaufman PL, Alm A, Levin LA, Adler FH. Adler's physiology of the eye. 11th ed. London, New York: Saunders/Elsevier; 2011.
12. Streilein JW. Ocular immune privilege: therapeutic opportunities from an experiment of nature. Nat Rev Immunol. 2003;3(11):879–89.
13. Zamiri P, Sugita S, Streilein JW. Immunosuppressive properties of the pigmented epithelial cells and the subretinal space. Chem Immunol Allergy. 2007;92:86–93.
14. Beeram M, Krop IE, Burris HA, Girish SR, Yu W, Lu MW, *et al*. A phase 1 study of weekly dosing of trastuzumab emtansine (T-DM1) in patients with advanced human epidermal growth factor 2-positive breast cancer. Cancer. 2012;118(23):5733–40.
15. Burris HA 3rd, Rugo HS, Vukelja SJ, Vogel CL, Borson RA, Limentani S, *et al*. Phase II study of the antibody drug conjugate trastuzumab-DM1 for the treatment of human epidermal growth factor receptor 2 (HER2)-positive breast cancer after prior HER2-directed therapy. J Clin Oncol. 2011;29(4):398–405.
16. Maker AV, Yang JC, Sherry RM, Topalian SL, Kammula US, Royal RE, *et al*. Intrapatient dose escalation of anti-CTLA-4 antibody in patients with metastatic melanoma. J Immunother. 2006;29(4):455–63.
17. Borkar DS, Lacouture ME, Basti S. Spectrum of ocular toxicities from epidermal growth factor receptor inhibitors and their intermediate-term follow-up: a five-year review. Support Care Cancer. 2013;21(4):1167–74.
18. Fraunfelder FT, Fraunfelder FW. Trichomegaly and other external eye side effects associated with epidermal growth factor. Cutan Ocul Toxicol. 2012;31(3):195–7.
19. Eaton JS, Miller PE, Mannis MJ, Murphy CJ. Ocular adverse events associated with antibody-drug conjugates in human clinical trials. J Ocul Pharmacol Ther. 2015;31(10):589–604.
20. Polat O, Inan S, Ozcan S, Dogan M, Kusbeci T, Yavas GF, *et al*. Factors affecting compliance to intravitreal anti-vascular endothelial growth factor therapy in patients with age-related macular degeneration. Turk J Ophthalmol. 2017;47(4):205–10.
21. Senra H, Balaskas K, Mahmoodi N, Aslam T. Experience of anti-VEGF treatment and clinical levels of depression and anxiety in patients with wet age-related macular degeneration. Am J Ophthalmol. 2017;177:213–24.
22. del Amo EM, Urtti A. Rabbit as an animal model for intravitreal pharmacokinetics: clinical predictability and quality of the published data. Exp Eye Res. 2015;137:111–24.
23. Short BG. Safety evaluation of ocular drug delivery formulations: techniques and practical considerations. Toxicol Pathol. 2008;36(1):49–62.
24. Zernii EY, Baksheeva VE, Iomdina EN, Averina OA, Permyakov SE, Philippov PP, et al. Rabbit models of ocular diseases: new relevance for classical approaches. CNS Neurol Disord Drug Targets. 2016;15(3):267–91.
25. Robinson GC, Jan JE. Acquired ocular visual impairment in children 1960–1989. Am J Dis Child. 1993;147(3):325–8.
26. Robinson GC, Jan JE, Kinnis C. Congenital ocular blindness in children, 1945 to 1984. Am J Dis Child. 1987;141(12):1321–4.
27 Amberger J, Bocchini CA, Scott AF, Hamosh A. McKusick's Online Mendelian Inheritance in Man (OMIM). Nucleic Acids Res. 2009;37(Database issue):D793-6.
28. Krebs MP, Collin GB, Hicks WL, Yu M, Charette JR, Shi LY, *et al*. Mouse models of human ocular disease for translational research. PLoS One. 2017;12(8):e0183837.
29. Won J, Shi LY, Hicks W, Wang J, Hurd R, Naggert JK, *et al*. Mouse model resources for vision research. J Ophthalmol. 2011;2011:391384.
30. Chang B. Mouse models for studies of retinal degeneration and diseases. Methods Mol Biol. 2013;935:27–39.
31. Chang B, Hawes NL, Hurd RE, Wang J, Howell D, Davisson MT, *et al*. Mouse models of ocular diseases. Vis Neurosci. 2005;22(5):587–93.
32. Herceptin(R). [package insert]. South San Fransisco, CA: Genentech, Inc. 1998.
33. Li Z, Li Y, Chang HP, Chang HY, Guo L, Shah DK. Effect of size on solid tumor disposition of protein therapeutics. Drug Metab Dispos. 2019;47(10):1136–45.
34. Singh AP, Sharma S, Shah DK. Quantitative characterization of *in vitro* bystander effect of antibody-drug conjugates. J Pharmacokinet Pharmacodyn. 2016;43(6):567–82.
35. Sharma S, Li Z, Bussing D, Shah DK. Evaluation of quantitative relationship between target expression and antibody-drug conjugate exposure inside cancer cells. Drug Metab Dispos. 2020;48(5):368–77.
36. Aerts J, Nys J, Arckens L. A highly reproducible and straightforward method to perform *in vivo* ocular enucleation in the mouse after eye opening. J Vis Exp. 2014;92:e51936.
37. SimBiology. 6.0 ed. Natick, Massachusetts, United States: The MathWorks, Inc.; 2020.
38. Nedelman JR, Gibiansky E, Lau DT. Applying Bailer's method for AUC confidence intervals to sparse sampling. Pharm Res. 1995;12(1):124–8.
39. Microsft Excel. Office 365. Redmond, Washington, United States: Microsoft Corporation; 2020.
40. Shah DK, Betts AM. Antibody biodistribution coefficients: inferring tissue concentrations of monoclonal antibodies based on the plasma concentrations in several preclinical species and human. MAbs. 2013;5(2):297–305.
41. Li Z, Krippendorff BF, Sharma S, Walz AC, Lave T, Shah DK. Influence of molecular size on tissue distribution of antibody fragments. MAbs. 2016;8(1):113–9.
42. Kazemi T, Tahmasebi F, Bayat AA, Mohajer N, Khoshnoodi J, Jeddi-Tehrani M, *et al*. Characterization of novel murine monoclonal antibodies directed against the extracellular domain of human HER2 tyrosine kinase receptor. Hybridoma (Larchmt). 2011;30(4):347–53.
43. Ding X, Gu W, Zhong Y, Hao X, Liu J, Xia S, *et al*. A novel HER2-targeting antibody 5G9 identified by large-scale trastuzumab-based screening exhibits potent synergistic antitumor activity. EBioMedicine. 2020;60:102996.
44. Jakubiak P, Alvarez-Sanchez R, Fueth M, Broders O, Kettenberger H, Stubenrauch K, *et al*. Ocular pharmacokinetics of intravitreally injected protein therapeutics: comparison among standard-of-care formats. Mol Pharm. 2021;18(6):2208–17.
45. Mordenti J, Cuthbertson RA, Ferrara N, Thomsen K, Berleau L, Licko V, *et al*. Comparisons of the intraocular tissue distribution, pharmacokinetics, and safety of 125I-labeled full-length and Fab antibodies in rhesus monkeys following intravitreal administration. Toxicol Pathol. 1999;27(5):536–44.
46. Drolet DW, Nelson J, Tucker CE, Zack PM, Nixon K, Bolin R, *et al*. Pharmacokinetics and safety of an anti-vascular endothelial growth factor aptamer (NX1838) following injection into the vitreous humor of rhesus monkeys. Pharm Res. 2000;17(12):1503–10.

47. Gaudreault J, Fei D, Rusit J, Suboc P, Shiu V. Preclinical pharmacokinetics of Ranibizumab (rhuFabV2) after a single intravitreal administration. Invest Ophthalmol Vis Sci. 2005;46(2):726–33.
48. Bakri SJ, Snyder MR, Reid JM, Pulido JS, Ezzat MK, Singh RJ. Pharmacokinetics of intravitreal ranibizumab (Lucentis). Ophthalmology. 2007;114(12):2179–82.
49. Bakri SJ, Snyder MR, Reid JM, Pulido JS, Singh RJ. Pharmacokinetics of intravitreal bevacizumab (Avastin). Ophthalmology. 2007;114(5):855–9.
50. Nomoto H, Shiraga F, Kuno N, Kimura E, Fujii S, Shinomiya K, *et al*. Pharmacokinetics of bevacizumab after topical, subconjunctival, and intravitreal administration in rabbits. Invest Ophthalmol Vis Sci. 2009;50(10):4807–13.
51. Gadkar K, Pastuskovas CV, Le Couter JE, Elliott JM, Zhang J, Lee CV, *et al*. Design and pharmacokinetic characterization of novel antibody formats for ocular therapeutics. Invest Ophthalmol Vis Sci. 2015;56(9):5390–400.
52. Sinapis CI, Routsias JG, Sinapis AI, Sinapis DI, Agrogiannis GD, Pantopoulou A, *et al*. Pharmacokinetics of intravitreal bevacizumab (Avastin(R)) in rabbits. Clin Ophthalmol. 2011;5:697–704.
53. Chang HY, Morrow K, Bonacquisti E, Zhang W, Shah DK. Antibody pharmacokinetics in rat brain determined using microdialysis. MAbs. 2018;10(6):843–53.
54. Mager DE, Jusko WJ. General pharmacokinetic model for drugs exhibiting target-mediated drug disposition. J Pharmacokinet Pharmacodyn. 2001;28(6):507–32.
55. Levy G. Pharmacologic target-mediated drug disposition. Clin Pharmacol Ther. 1994;56(3):248–52.